JOURNAL OF CATALYSIS 106, 483–493 (1987)

Microstructural Studies of Pt/C Catalysts for Hydrogenation of Nitric Oxide in Sulfuric Acid

S. POLIZZI, A. BENEDETTI, AND G. FAGHERAZZI

Dipartimento di Chimica Fisica, Università di Venezia, Venice, Italy

S. FRANCESCHIN, C. GOATIN, AND G. TALAMINI

Centro Ricerche Montedipe, Porto Marghera, Venice, Italy

AND

L. TONIOLO

Dipartimento di Chimica Inorganica, Metallorganica ed Analitica, Università di Padova, Padua, Italy

Received October 28, 1985; revised January 27, 1987

Pt/charcoal catalysts with platinum contents in the range 1.2–11.3 wt%, as used in a slurry reactor for the production of hydroxylamine by hydrogenation of nitric oxide in a sulfuric acid environment, have been microstructurally characterized by small angle X-ray scattering, line-broadening analysis of wide angle X-ray scattering profiles, and transmission electron microscopy. The microstructural data are related to the results of chemisorption analysis and to the catalytic rates of hydroxylamine production, giving a better insight into the catalytic process. © 1987 Academic Press, Inc.

1. INTRODUCTION

The synthesis of hydroxylamine, an intermediate in the production of ε-caprolactam, via catalytic hydrogenation of nitric oxide, is of considerable interest because of its industrial importance as an alternative process to the Raschig reaction (*1*).

The scientific literature on this reaction has recently been reviewed by Tauszik and Crocetta (*2*), who also carried out an interesting attempt to match electrochemical and catalytic approaches to the problem. Most of the studies deal with platinum-on-carbon catalysts suspended in a vigorously stirred aqueous sulfuric acid solution and are carried out under mild temperature conditions.

A systematic study of the kinetics of the reaction has been published by Temkin and co-workers (*3*), who proposed a mechanism for the reaction and derived the related kinetic equations. However, a lack in the microstructural characterization of these Pt/C catalysts is felt throughout the whole literature on the subject. The aims of the present work are to fill this gap and to support the interpretation of the catalytic performances to be reported in the following paper (*4*).

2. EXPERIMENTAL

Measurements were carried out on four Pt/C catalysts containing respectively 1.2 wt% (I), 3.0 wt% (II), 5.6 wt% (III), and 11.3 wt% (IV) of platinum dispersed on a Lurgi KE active carbon and prepared by reduction of K_2PtCl_4 in aqueous acid solution at 70–100°C (*4*). The specific surface area of the carbon support is 978 m^2/g, as measured by BET, and 1015 m^2/g by small angle X-ray scattering.

0021-9517/87 $3.00

2.1. *Small Angle X-Ray Scattering (SAXS)*

SAXS data were collected with a Paar compact Kratky camera, using Zr-filtered Mo$K\alpha$ radiation and a scintillation counter with fixed counting statistics of 10^5 pulses per point.

In order to eliminate interferences due to electron density heterogenities arising from the pores of the charcoal particles, the "pore-maskant" method (*5*) was used. $C_2H_4Br_2$, which has an electron density very close to that of the support, was introduced into the porous phase by impregnation, following a technique reported elsewhere (*6*).

SAXS methods and equations used for experimental data processing are reported in Section 3.1.

2.2. *Wide Angle X-Ray Scattering (WAXS) for Line-Broadening (LB) Analysis*

WAXS measurements were carried out in order to perform LB analysis on the available X-ray diffraction peaks originating from the fcc lattice of Pt(111, 200, 222, 400).

Ni-filtered Cu$K\alpha$ radiation and a step-by-step technique were employed (steps of 0.02° and 4×10^4 pulses per angular abscissa) on a powder X-ray diffractometer, equipped with a graphite focusing monochromator and a scintillation counter.

The procedure for LB analysis and equations used for experimental data processing are reported in Section 3.2.

2.3. *Transmission Electron Microscopy (TEM)*

Bright-field high-resolution microscopy was carried out using a Philips EM200 electron microscope with accelerating potential of 60 kV. Condenser aperture and other parameters were adjusted in order to achieve a resolution of about 10 Å. Specimens were prepared with conventional methods including suspension in polymethylmethacrylate (PMMA) and sectioning with an ultramicrotome (LKB Model 8800) fitted with a diamond knife.

3. METHODS

3.1. *Outline of SAXS Theory and Experimental Data Processing*

Recently, a new approach to the study by SAXS of a multiphase system has been developed and applied to Pt/Al_2O_3 catalysts (*7*). This method, based on the parameterization of correlation functions relevant to all the pairs of different phases, allows an estimate of the interphase irregularities (i.e., the angularities of the interfaces) (*8*). Furthermore, it is possible to see which of the possible assumptions as to the relative geometrical configurations of the support and the metallic phase, is the most appropriate to the sample under examination.

However, in order for this approach to be safely applied, the experimental intensity curve should follow the Porod law. Since the present system shows a positive linear deviation from the Porod law, we have applied the well-known "pore-maskant" method (*5*). In this way, in spite of the implicit assumption of addition of the scattering intensity due to the metal to that due to the support and of objective difficulties in the treatment of the experimental data, reliable information about the dispersed metal particle can be obtained (*9*).

The metal specific surface (SS) can be derived from the asymptotic value in the tails of SAXS intensity curve according to the Porod relation (*10*):

$$SS_P^{SAXS} = 4\frac{\phi_1\phi_2}{d_B}\frac{K \times 10^4}{\int_0^\infty J(h)hdh}(m^2/g), \quad (1)$$

where $h = 4\pi\sin\theta/\lambda$, 2θ is the scattering angle, and λ is the X-ray wavelength employed; $J(h)$ is the slit smeared scattered intensity; Φ_1 and Φ_2 are the volume fractions of the metallic particles and that of the support or matrix (charcoal plus pores in the present case), respectively; d_B (g/cm^3)

is the bulk density of the system and $K = \lim_{h\to\infty} h^3 J(h)$ is the Porod constant.

It is possible to obtain an average dimension of the scattering particles (Porod diameter) by applying Eq. (2) (*10*):

$$D_P^{SAXS} = \frac{3}{2\phi_2} \frac{\int_0^\infty J(h)hdh}{K}. \quad (2)$$

The volumetric distribution $\rho_V^{SAXS}(D)$ of the particle diameters can be deduced, in the hypothesis of spherically shaped particles, using a Titchmarsh transform (*11*) of the scattered slit smeared intensity $J(h)$ as

$$\rho_V^{SAXS}(D) \propto D \int_0^\infty [h^3 J(h) - K] \cdot [2J_0(hD) + J_1(hD)(hD - 3/hD)]\, dh, \quad (3)$$

where J_0 and J_1 are the first kind Bessel functions of zero and first order.

Using this function it is possible to derive another value for the specific surface

$$\langle SS\rangle^{SAXS} = \frac{6}{d_B} \int_0^\infty \frac{\rho_V^{SAXS}(D)}{D}\, dD \quad (4)$$

and for the average particle diameter

$$\langle D\rangle^{SAXS} = \int_0^\infty \rho_V^{SAXS}(D) D dD \quad (5)$$

with the normalization condition: $\int_0^\infty \rho_V^{SAXS}(D)\, dD = 1$.

The percentage exposed or dispersion D_S, defined as the ratio of the number of surface atoms to the number of total atoms, can be calculated assuming a spherical shape of the particle as

$$D_S = \int_0^\infty \frac{D^3 - (D - 2d_0)^3}{D^3} \rho_V^{SAXS}(D) dD, \quad (6)$$

where d_0 is the atomic diameter of platinum (monolayer approximation).

3.2. Procedures for X-Ray Line-Broadening Fourier Analysis

The procedure for data processing refers to the Warren-Averbach (W-A) method (*12*), combined with Stokes' formulas (*12*) for deconvolution of experimental factors and preceded by a best fit of X-ray peak profiles following a technique recently proposed by some of the present authors (*13*).

The fitting procedure enables the W-A Fourier analysis to be carried out even in cases (like the present one) in which a severe overlapping of peaks and/or an important and complex background are present. The better background subtraction and the consequent better evaluation of peak tails also drastically reduces the so-called "hook" effect in Fourier coefficients (*12*).

In the present paper the method is further tested by carrying out a deeper comparison of different forms of analytical functions, either symmetrical or asymmetrical. On the basis of earlier literature (*14*), two different analytical functions have been tested here in order to simulate ordinary diffraction symmetrical peaks: a pseudo-Voigt function (linear combination of a Gaussian profile with a Cauchian one) and a Pearson VII function. From the physical point of view, the pseudo-Voigt function seems to be more meaningful in respect to the Pearson VII for the following reasons: (1) it preserves a strict relation to the Gaussian or Cauchian nature of the peak often associated with physical properties (*15*); (2) it follows, on the tails, the law $\lim_{s\to\infty} I(s)s^2 =$ constant, which has been theoretically foreseen by Allegra (*16*) and experimentally confirmed by various authors (*17*).

In the procedure used, the α_1–α_2 doublet is taken into account by using a sum of two pseudo-Voigt or Pearson VII functions per peak and the well-known crystallographic constraints (*12*) on peak intensities, angular positions, and half-width at half-maximum. In this way, the parameters of the function relative to the α_1 peaks are automatically obtained and can be used in subsequent analysis. The introduction of a further term accounting for the α_3 satellite group (*18*) together with other instrumental grounds of asymmetrization has been demonstrated to

be useful only in cases of very narrow peaks (e.g., reference peaks) at relatively low angles (up to ≅35°) (*13*). A linear expression is usually used for the background. The minimization of the sum of the squares of the differences between observed and calculated values of the intensities is carried out by the simplex method (*19*). The criterion used for the goodness of fit (GOF) is defined as

$$\mathrm{GOF} = \left(\frac{\sum_{i=1}^{n} [I_i(\mathrm{obs}) - I_i(\mathrm{fit})]^2}{\sum_{i=1}^{n} [I_i(\mathrm{obs})]^2} \right)^{1/2}$$

which, according to Young and Wiles (*15*), is the most meaningful indicator of overall fit.

Owing to the scarcity of literature in this field it seemed useful to compare the different functions used here in terms of GOF. As can be seen in Table 1, pseudo-Voigt and Pearson VII functions are both adequate from the GOF point of view. On the basis of the previously discussed physical arguments, the pseudo-Voigt function was chosen in order to obtain the final results (i.e., ρ_V^{LB} and $\langle D \rangle^{LB}$) reported below. Moreover, in the present case, besides small $CaCO_3$ contributions that were initially smoothed out, a prominent "background" due to the (*hk*) broad peaks of the poorly graphitized carbon used for the catalyst support is also present. This gives rise to asymmetric peaks in the neighborhood of the peaks of interest relevant to platinum (see, for example, Fig. 2).

TABLE 1

Goodness of Fit[a] (%) (GOF) Using Different Functions

Sample	Pt peaks		Carbon peak		Nothing[b]
	p-Voigt	Pearson VII	Maxwell	n-log	
I	0.9	1.0	2.2	0.9	—
III	1.8	1.7	1.7	2.0	2.1
IV	1.5	1.6	1.5	1.8	1.9

[a] Fit of envelope A (see Fig. 1a); testing the function for Pt peaks, the one for carbon was chosen as the best for that sample, and vice versa.

[b] Fit obtained neglecting the carbon contribution; this is not possible for sample I, where the carbon peak is very intense.

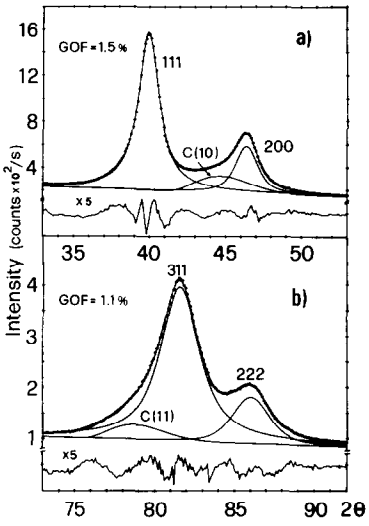

FIG. 1. Experimental data (dots) and fitting (continuous line) of four reflections from sample IV (Pt 11.3 wt%). (a) Envelope A (111 and 200 platinum lines, and 10 carbon line); (b) Envelope B (311 and 222 from platinum lines, and 11 from carbon). Residuals (differences between experiment and fit) are reported below on a 5× magnified scale.

The peak envelopes of interest are Pt(111) + C(10) + Pt(200) (envelope A; see for example Fig. 1a); Pt(311) + C(11) + Pt(222) (envelope B; see, for example, Fig. 1b); and the rather isolated but very low 400 peak.

In order to fit carbon peaks, two different asymmetric functions were tested: these were a Maxwellian function and a normal–logarithmic one (both calling for four adjustable parameters, just like pseudo-Voigt and Pearson VII functions). A comparison between the different functions in terms of GOF is reported in Table 1 for the envelope A fitting for samples I, III, and IV. The normal–logarithmic function behaves better than the Maxwellian one for sample I, where the carbon peak is very important, while the opposite happens for samples III and IV. In fact, the analytical

form for carbon peaks proposed by Warren (*20*) on physical grounds could be used; this is, however, computationally very time consuming and for the present purposes the two functions already utilized seem to us satisfying.

The approach discussed above has also allowed reliable processing of the present experimental data in some critical cases as, for example, the analysis of the 111 peak of sample I (Fig. 2), where the "graphitic background" was predominant, that of the 222 peak (Fig. 1b), heavily overlapped with other prominent peaks, and that of the very weak 400 reflection (not shown).

The disorder analysis was carried out on samples III (111–222) and IV (111–222 and 200–400 pairs). No disorder was detected, as can be seen, for example, in Fig. 3.

3.3. TEM Method for Observation of Very Fine Pt Particles

Although the resolution of the instrument is of the order of 10 Å, factors like the thickness of the sample may, in the case of carbon used as catalyst support, obscure the presence of very fine particles or make their assignment uncertain. In this case, it is difficult to detect metal particles smaller than about 20 Å (*21*).

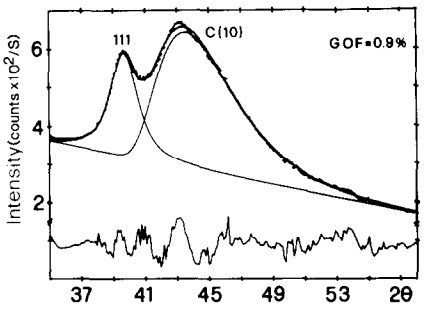

FIG. 2. Experimental data (dots) and fitting (continuous line) of envelope A from sample I (Pt 1.2 wt%). Residuals are reported below on a 5× magnified scale. For this sample the 200 peak is completely hindered by the "background"; the fitting procedure has shown that it can be disregarded.

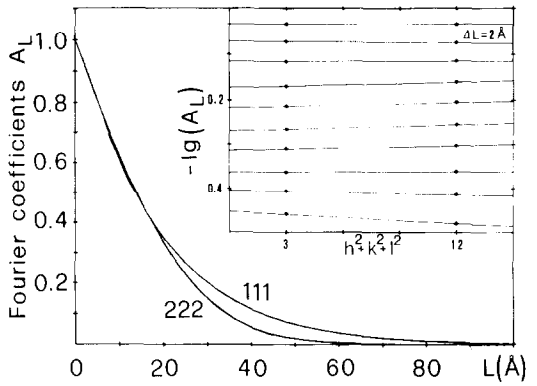

FIG. 3. A_L Fourier corrected (by Stokes' procedure) coefficients for the 111–222 pair of reflections computed from the analytical forms reported in Fig. 1. Inset: Warren–Averbach diagram in which the logarithms of A_L are reported as functions of $(h^2 + k^2 + l^2)$, with h, k, l Miller indexes. From the slope of the straight lines, the strain parameter can be obtained. In the present case it is zero. The volume distribution for the crystallite diameters $\rho_V^{LB}(D)$ is obtained from the equation $\rho_V^{LB}(D) = D(d^2A_L(L)/dL^2)_{L=D}$, and the average diameter values $\langle D\rangle^{LB}$ are obtained from the equation $\langle D\rangle^{LB} = \int_0^\infty \rho_V^{LB}(D)DdD$.

In order to bypass this difficulty, a new preparation method, based on that of Krakow and Howland (*22*), was used. The method consists in allowing a different metal to be grown around the metal particles present in the catalyst, thus making it possible to detect the original ones.

Activation of the metal phase by reduction in H_2 and subsequent decomposition of copper formate, i.e., $Cu(OOCH)_2 \rightarrow Cu + 2CO_2 + H_2$, has been demonstrated to give the best results (*23*).

Figure 4 shows samples I and III before and after the preparation described above. It can be seen that very fine particles are shown up by this treatment (no effect was detected on a specimen without platinum). Although the method is very useful for localizing very fine particles, it is worth noting that the information about their diameters is lost after the treatment (only an upper limit of about 20 Å for particles not visible before the treatment is possible).

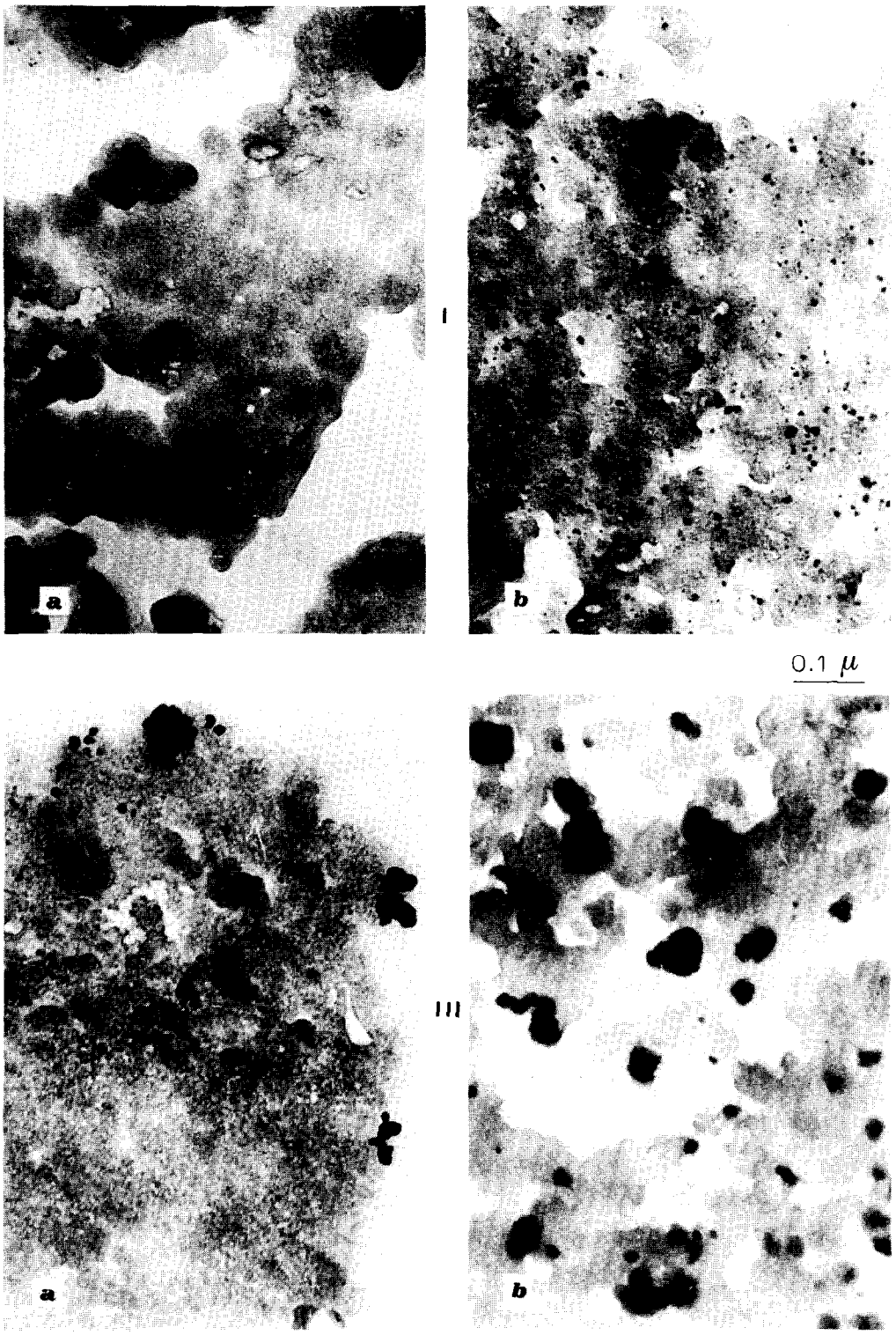

FIG. 4. TEM pictures of sample I (1.2 wt%, top) and III (Pt 5.6 wt%, bottom) before (a) and after (b) the treatment (see text) carried out in order to show up very fine platinum particles.

4. RESULTS

Figure 5 shows the normalized volumetric distributions $\rho_V^{LB}(D)$ of metallic crystallite diameters obtained by the X-ray diffraction line-broadening analysis following the methods described in Section 3. The average diameter values, $\langle D\rangle^{LB}$, calculated perpendicularly to the (111) planes, are reported in Table 2. It is interesting to observe that the crystallite dimensions are practically the same for the four catalysts investigated, in spite of the different Pt concentrations.

Figure 6 shows the normalized volumetric distribution curves $\rho_V^{SAXS}(D)$ obtained by SAXS on the four supported catalysts investigated for the metallic particle diameters using Eq. (3). The average particle diameters, $\langle D\rangle^{SAXS}$, obtained from $\rho_V^{SAXS}(D)$ by Eq. (5), as well as the Porod diameters D_P^{SAXS} deduced by Eq. (2), are reported in Table 2. The particle size of Pt slightly increases on raising the metal content, the largest difference being observed between catalyst IV and the others. The specific surface of the metal phase $\langle SS\rangle^{SAXS}$ and the dispersion D_S^{SAXS}, related to $\rho_V^{SAXS}(D)$ by Eqs. (4) and (6), behave accordingly (see Table 3).

TABLE 2

Average Crystallite and Particle Diameters of Platinum

Sample	$\langle D\rangle^{LB}$[a] (Å)	$\langle D\rangle^{SAXS}$[b] (Å)	D_P^{SAXS}[c] (Å)
I	38	38	16
II	40	41	19
III	40	49	23
IV	38	74	45

[a] From WAXS crystallite size distribution obtained by line-broadening (LB) analysis using the 111–222 X-ray reflections. Error can be evaluated as 20%.

[b] From SAXS particle size distribution. Error can be evaluated as 20%.

[c] From Porod theory.

It is worth noting that the D_P^{SAXS} and SS_P^{SAXS} values, obtained with the Porod theoretical approach, closely follow the trend of the corresponding values D^{SAXS} and $\langle SS\rangle^{SAXS}$, worked out by averaging the $\rho_V^{SAXS}(D)$ distributions. Only the scale is different: Porod diameters are, as is usually the case (*6, 9, 10*), smaller than the averaged ones.

Finally, the last two columns of Table 3 report the chemisorption specific surfaces,

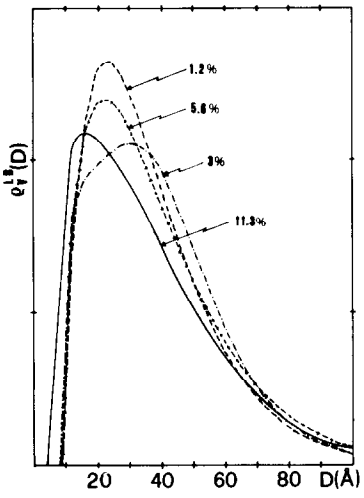

FIG. 5. Particle size distributions obtained by line-broadening analysis of WAXS profiles: samples I (---); II (-·-); III (-+-); and IV (—).

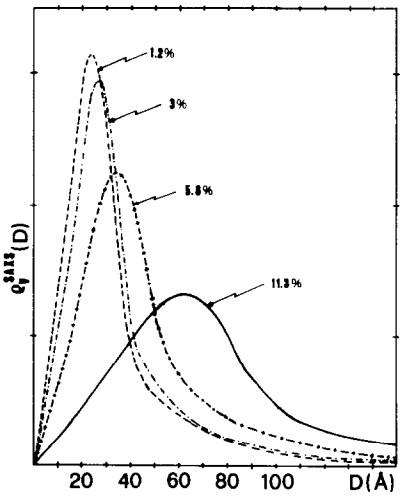

FIG. 6. Particle size distributions obtained by SAXS: samples I (---); II (-·-); III (-+-); and IV (—).

TABLE 3

Specific Surface Areas and Dispersions

Sample	$\langle SS\rangle^{SAXS}$[a] (m^2/g Pt)	D_S^{SAXS}[a]	SS_P^{SAXS}[b] (m^2/g Pt)	SS^{CHEM}[c] (m^2/g Pt)	D_S^{CHEM}[c]
I	131	0.68	171	118	0.54
II	119	0.63	149	49	0.26
III	93	0.49	123	25	0.14
IV	55	0.30	61	—	—

[a] From SAXS particle size distribution.
[b] From Porod theory.
[c] Titration with H_2 of preadsorbed oxygen at room temperature.

SS^{CHEM}, measured by titration with H_2 of preadsorbed oxygen at room temperature (data from Ref. (*2*)) and the dispersion D_S^{CHEM} obtained from SS^{CHEM} in the hypothesis of spherically shaped metal particles.

Figure 7 shows some TEM micrographs, one for each catalyst investigated, from which it might be argued that only catalyst I has a completely well-dispersed metallic phase while the others contain large metal agglomerates (up to sizes of thousands of Å) and only a few fine particles of 20–40 Å. However, the technique described in Section 3.3 showed the presence of a background of very fine particles, smaller than about 20 Å, in all the catalysts (see Fig. 4). Furthermore, although the TEM micrographs of catalysts II, III, and IV show platinum to agglomerate progressively, a careful examination finds that these agglomerates have indented borders, actually suggesting a heap of particles of about 50 Å, more than large single particles. This fine microstructure can also be observed in the body of some agglomerates when they have a partial transparency with respect to the electron beam.

5. DISCUSSION

The microstructural data reported in the previous section suggest a three-level metal phase subdivision:

(1) *crystallites,* the majority of which have diameters in the range 15–40 Å, present in all the catalysts;

(2) *particles,* made up of one or a few crystallites, with average diameters ranging from about 40 Å (sample I) to 75 Å (sample IV);

(3) *agglomerates* of particles with a size ranging from about 100 to about 2000 Å and apparently very porous.

The fact that the dimension of the basic constituent bricks (i.e., the crystallites) are the same for all the catalysts gives an insight into the process of formation of metal particles by the chemical method of preparation utilized (a standard one). It is likely that at the beginning of the process the precipitation of a small percentage of platinum (less than or about 1.5 wt%) gives rise to the growth of very fine crystallites of nearly the same size on active nuclei of the support, whatever the global metal content. A further precipitation gives rise to a process of gradual agglomeration of particles, more than to a further increase in size. These agglomerates should be situated at the outer core of the carbon particles, as also shown by TEM, while the very fine initially deposited crystallites are very likely to be homogeneously distributed over the total volume of the support particles.

The three-level view outlined above has the following implications:

The $\langle SS\rangle^{SAXS}$ values (as well as the SS_P^{SAXS}) should decrease more slowly than the corresponding SS^{CHEM} values as the platinum concentration increases because the SS^{CHEM} values concern just the "external" (i.e., "exposed" to the oxygen) specific surface of the metallic phase, while the $\langle SS\rangle^{SAXS}$ values refer to the "total" specific surface of the same phase as "seen" by the totally penetrating X-rays.

The well-dispersed very fine particles present in all the samples should be the catalytically active sites, while the amount of platinum over 1.5 wt% will probably be

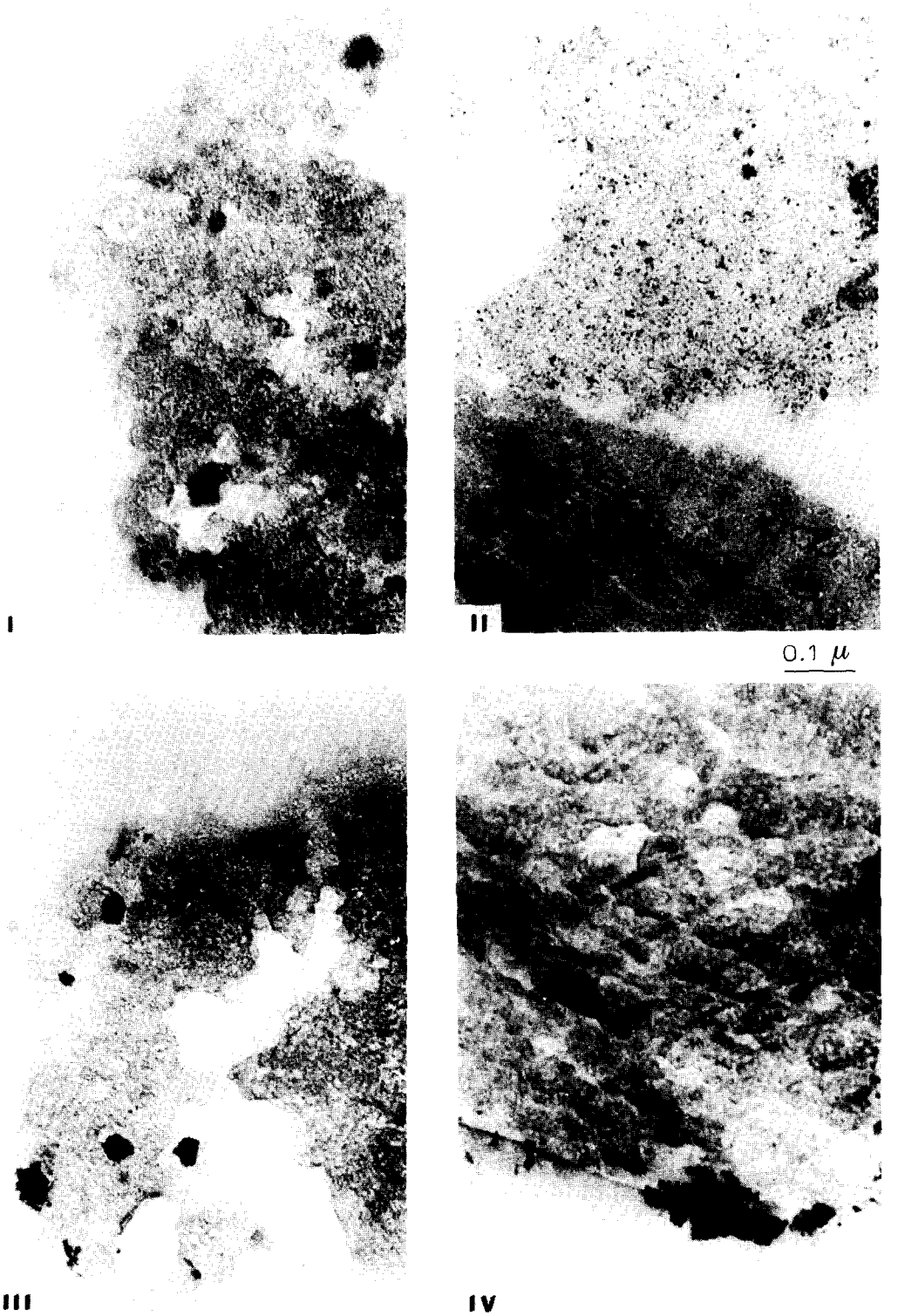

FIG. 7. TEM pictures of sample I, II, III, and IV as indicated.

of minor importance due to the strong agglomeration effect.

As shown in Table 3, the first implication is really verified, thus confirming the greater and greater particle agglomeration as the platinum percentage increases, qualitatively observed by TEM (the difference between $\langle SS \rangle^{SAXS}$ and SS^{CHEM} for sample I is probably within the error limit of these two very different techniques).

The second implication is that the use of large platinum concentrations, besides being economically unprofitable, is probably not even effective in this type of supported metal catalyst. This has found very good confirmation in the total NO consumption values as a function of the platinum content in the catalyst (see Table 4), obtained in experiments such as those described in the following paper (*4*). The consumption of NO, referred to a fixed amount of Pt (e.g., 1 g), drastically decreases as the Pt wt% increases.

In Table 4, the values of the turnover number N^{SAXS} and N^{CHEM}, calculated as the number of NO molecules reacted per Pt atom exposed and per second (from the dispersion values reported in Table 3), are also indicated. From the catalytic point of view, the N^{CHEM} values are obviously more realistic than the N^{SAXS} values, the N^{CHEM} values being based on the "exposed" surface area. The rather constant value of N^{CHEM}, within the error limit, indicates the absence of a structure sensitivity of the present reaction, at least for particles which are not extremely fine like those involved in the present catalysts.

TABLE 4

Total NO Consumption and Turnover Numbers[a]

Sample	Total NO consumption (g NO/g Pt h)	N^{SAXS}	N^{CHEM}
I	92.6	0.279	0.35
II	35.6	0.118	0.29
III	18.1	0.077	0.27
IV	11.8	0.078	—

[a] Running conditions: P_{NO} = 0.06 atm, P_{H_2} = 0.56 atm, T = 40°C.

6. CONCLUSIONS

A systematic study of catalytic performances of samples with increasing metal surface area would be crucial in order to understand the role played by liquid–solid mass transport phenomena in the reaction under examination. Unfortunately, the present work has demonstrated that such an ad hoc set of samples is not at all easy to prepare. We found that a standard preparation method is in fact able to produce well-dispersed small platinum particles ($\lesssim$25 Å) in the carbon matrices for a metal content of 1.2%, but is not able to avoid the process of increasing agglomeration of the particles with greater content of the metal phase. This suggests that the study of the above-mentioned transport phenomena should be carried out on a set of samples with metal contents lower than or about 1.5 wt%. However, a microstructural characterization of such samples would be much more difficult, at least with the techniques used in the present work.

Finally, our results show that the use of a small platinum content ($\leq$1.5 wt%) is more adequate for industrial purposes, a greater quantity being ineffective for the reaction, as already suggested in a similar case by Renouprez *et al.* (*24*).

ACKNOWLEDGMENT

This work was partly supported by the Italian Ministry of Education (MPI 40%).

REFERENCES

1. van de Moesdijk, C., *Polytechnisch Tijdschrift, Procestechniek* **36,** 199 (1981); van de Moesdijk, Doctorate thesis, Technische Hogeschool Eindhoven, 1979, pp. 143–171.
2. Tauszik, G. R., and Crocetta, P., *Appl. Catal.* **17,** 21 (1985).
3. Lopatin, V. L., Kul'kova, N. V., and Temkin, M. I., *Kinet. Catal.* (Engl. ed.) **23,** 726 (1982), and references therein.

4. Polizzi, S., Benedetti, A., Fagherazzi, G., Goatin, C., Strozzi, R., Talamini, G., and Toniolo, L., *J. Catal.* **106,** 494 (1987).
5. White, T. E., Jr., Kirklin, P. W., Gould, R. W., and Heinemann, H., *J. Catal.* **25,** 407 (1972).
6. Fagherazzi, G., Cocco, G., Schiffini, L., Enzo, S., Benedetti, A., Passerini, R., and Tauszik, G. R., *Chim. Ind. (Milan)* **60,** 892 (1978).
7. Ciccariello, S., and Benedetti, A., *J. Appl. Crystallogr.* **18,** 219 (1985).
8. Ciccariello, S., *J. Appl. Phys.* **56,** 162 (1984).
9. Cocco, G., Enzo, S., Fagherazzi, G., Schiffini, L., Bassi, I. W., Galvagno, S., and Parravano, G., *J. Phys. Chem.* **83,** 2527 (1979).
10. Porod, G., *in* "Small Angle X-Ray Scattering" (O. Glatter and O. Kratky, Eds.), p. 32. Academic Press, New York, 1982.
11. Fedorova, I. S., and Schmidt, P. W., *J. Appl. Crystallogr.* **11,** 405 (1978).
12. Warren, B. E., "X-Ray Diffraction," Addison–Wesley, Reading, MA, 1969; Wagner, C. N. J., *in* "Local Atomic Arrangements Studied by X-Ray Diffraction" (J. B. Cohen and J. E. Hilliard, Eds.), pp. 219–268. Gordon & Breach, New York, 1966.
13. Enzo, S., Polizzi, S., and Benedetti, A., *Z. Kristallogr.* **170,** 275 (1985).
14. Young, R. A., and Wiles, D. B., *J. Appl. Crystallogr.* **15,** 430 (1982).
15. Mitra, G. B., *J. Appl. Phys.* **16,** 77 (1965); Ruland, W., *J. Appl. Crystallogr.* **1,** 90 (1968); Langford, J. I., *J. Appl. Crystallogr.* **11,** 10 (1978).
16. Allegra, G., *Acta Crystallogr. Sect. A* **38,** 863 (1982).
17. Szanto, I. S., and Varga, L., *J. Appl. Crystallogr.* **2,** 72 (1969); Enzo, S., and Parrish, W., *in* "Advances in X-Ray Analysis" (J. B. Cohen *et al.*, Eds.), vol. 27, p. 37. Plenum, New York, 1984.
18. Langford, J. I., *J. Appl. Crystallogr.* **1,** 48 (1968).
19. Nelder, J. A., and Mead, R., *Comput. J.* **7,** 308 (1965).
20. Warren, B. E., *Phys. Rev.* **59,** 693 (1941).
21. Millward, G. R., *J. Catal.* **64,** 381 (1980).
22. Krakow, W., and Howland, L. A., *Ultramicroscopy* **2,** 53 (1976).
23. Franceschin, S., and Zenoni, G., "Montedipe Internal Report (Porto Marghera)," n. 17584, 1984.
24. Renouprez, A., Hoang-Van, C., and Compagnon, P. A., *J. Catal.* **34,** 411 (1974).